International Journal of Advanced Science and Technology
Vol. 29, No. 11s, (2020), pp. 909-920

Reliability Anlaysis of Autism spectrum disorder in Amygdala domain using Asperger's syndrome

R. Lalitha,
Research Scholar, Bharathiar University, Coimbatore, Tamil Nadu
Dr. J. Jebamalar Tamilselvi
Research Guide &Professor, Department of CSE, Jaya Engineering College, Chennai, Tamil Nadu

Abstract

Autism spectrum disorder is a mental disorder that is found Children. The main cause and symptoms of this cause are Asperger's Syndrome and are being investigated in this area. Many medical techniques such as fMRI scans and DSM-V Used to identify gestures. A renowned and trusted technology, simultaneously, benefits from Autism. Previous research paper the frequency, this feature is cached using Amygdala domain properties and domain properties over time are acquired Usage of these features provided as input sushisen algorithm using Drosophila and CNN classification results were compared get the best rating for the system time domain. Subspace accuracy gave the highest accuracy using 94.46% and Sensitivity 96.52%. Frequency domain provided the second best 94.88% results using CNN rating. Because of the popularity of spending and spending time. Although ASA This analysis is not well known because the micro-voltages of the signal contain small portions and high volumes. This paper, research is being done to promote noise of Asperger's Syndrome . Autism is being tested using supported software datasets were obtained for 20 general patients from UCI and 10 autistic patients from NIAK 2020.The dataset was already processed using FIR and HH filters. This FIR filter used higher order FIR but physically it was hard to feel filter Butterworth, Chebyshev, and Elliptic filters provided the best can be used to implement results and hardware. Time and frequency domain features extraction. This may be because the frequency is lower than the domain with the increasing number of utilities. The test was made dataset can perform the same procedure in real time determine accuracy using fMRI scans System. The results can be further improved new algorithms implementation well-known HFA technique using improved reliability 96.33% better results.

Keywords: Autism spectrum disorder, Amydala domain, Butterworth, Chebyshev, frequency, Asperger's Syndrome.

INTRODUCTION

Lack of quality of social interaction, limited recall and negative attitudes, interests and activities. Dementia causes medically necessary disability in other important areas of the community, profession or occupation. Words used for children 2 years old, communication sentences 3 years old). There are no significant health delays other than social interaction and interest in cognitive development or the development of age-appropriate self-help abilities about the atmosphere of childhood.

Attention-deficit / hyperactivity disorder (ADHD) is a chronic neurodegenerative disorder that affects about 5% of children. Reduce symptoms, but often unsatisfactory side effects and failure to prevent or change long-term course ADHD symptom severity has been linked to decreased consumption of processed foods, food dyes, and fruits and vegetables. 3 Recent meta-analyzes 4 and literature review 5 indicate the role of diet and the benefits of manipulation of food in the expression of ADHD symptoms. In curing these symptoms. However, food handling can be a challenge for some families, supplemented with more nutrients than an alternative Which is available only through food. Therefore, dietary supplements in the form of additional micronutrients provide an alternative to traditional medical approaches and provide another option for children who do not respond to conventional treatment.

Those who experience adverse side effects associated with the drug. There is a growing body of evidence for a broad spectrum microcirculation approach with case studies, open label reverse design and randomized controlled trials, all documenting its therapeutic benefits.

Approach 6 a double-blind, randomized, placebo-controlled trial (RCT) from our own partner showed a significant benefit of micronutrients over placebo for normal functioning, emotional dissociation, aggression, and inattention. There were no group differences

Exponential / Impulsive. Children with ADHD exhibit significant neurological abnormalities, especially the striatum and frontal, compared to older adults. This reflects the quality of many aspects of the child's environment, including the risk level of chronic stress. Low SES families have more children

REVIEW OF LITERATURE

Many tensions are likely to occur, including neighborhood violence, chaotic homes and family upheavals (Evans and Kim, 2013). It is theorized that poverty-related stress affects hypothalamic - pituitary - adrenal axonal stress and alters the development of brain structures with high concentrations of glucocorticoid receptors, such as the amygdala (Naughty et al., 2012). . Several structural neuroimaging studies have shown a relationship between socioeconomic factors and amygdala levels in children, but not A.

The discrepancy of unions is uneven. Two studies have found that socioeconomic disadvantage may be associated with lower levels of amygdala (Hanson et al., 2015; Luby).

Et al., 2013, while another found that it could be associated with larger amygdala volumes (Noble et al., 2012). Other studies have failed to detect significant SES-related differences in amygdala structure in children (Hanson, Chandra, Wolff, & Pollak, 2011; Noble et al., 2015).

The proposed method makes abounding use of the advantage of FCN (Bin Fang.,et al. 2019) to automatic localization and deformable archetypal to clarify the surface. The deformable archetypal is acquired from NMF and apprenticed by LCSH. Experimental after-effects on dispensary abstracts approved the robustness of the proposed adjustment to noise, low adverse and heterogeneity (Zhang J., et al. 2017). The after-effects are satisfactory and aggressive to state-of-the-art. We assured that the proposed adjustment is a able adjustment for automated Neuron segmentation.

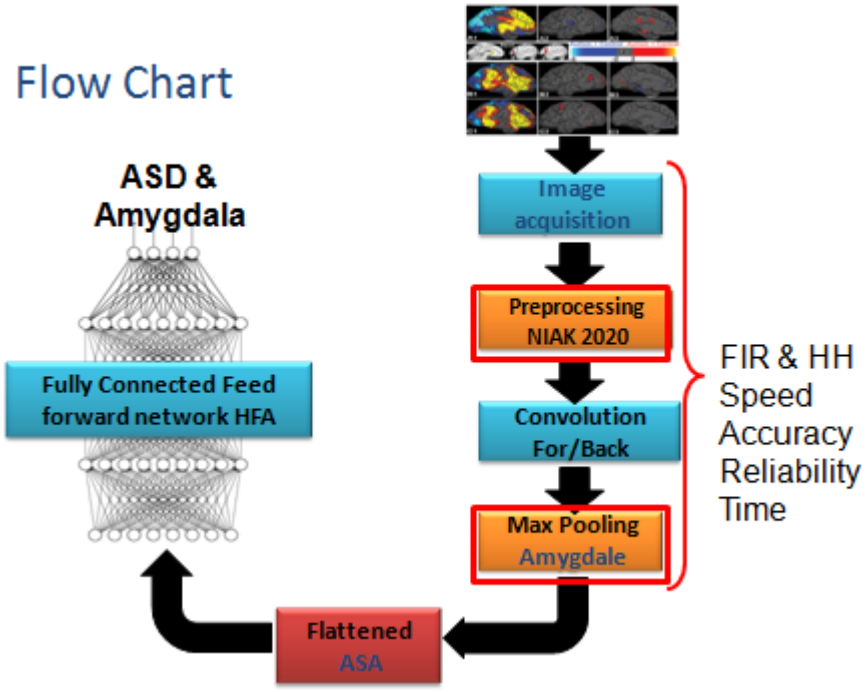

Fig 1: Autism spectrum disorder in amydala domain ASD reliability Anlaysis

ALGORITHMS

1. Input_shade(X1,X2,X3,Y1,Y2,Y3) Convolution
2. Splite dataset 25X25X25 =tmp <- round(overall, digits = digits)
3. Maxpooling 25X9= digits = max(3, getOption("digits") - 3),
4. Output full connected feed forward connection (MaxP,SD)
5. Init processing =print (Stats = TRUE, FALSE)

6. Sentence metric →Flattened
7. Frequency direction = Measure→AlphaGO
8. Feature _Map=(Softmax +if(is.null(mode))
9. stop(sensible _specify + precion _ recall +everything)
10. confusion Matrix <- function(x, mode =True),
11. tmp <- round(overall, digits = digits)
12. pIndex <- grep PValue names(overall)
13. tmp<- format.pval[overall[pIndex],
14. digits = digits overall <- tmp
15. ACCURACY <- overallText <- c(paste(overall["Accuracy"]),
16. Overall [c AccuracyNull, AccuracyPValue),
17. overall[McnemarPValue])
18. Frequency direction(dim(xtable)[1]>2
19. cat(Overall Statistics)
20. OverallNames<- if else(overallNames == paste(overallName))
21. out <- cbind (format(overallNames, justify = right< overallText)
22. colnames (out) <- rep(ncol (out))
23. rownames (out) <- rep(nrow(out))
24. Print(out, quote = FALSE)
25. Mode == (precision_recal ,sensible_specify)
26. if(mode ==prec_recall)
27. Class <- xbyClass[!grepl((Sensitivity)|(Specificity)|(Pos->Pred Value)
28. Neg Pred Value=names(byClass))]
29. if(mode ==sens_spec)
30. xbyClass <- xbyClass[!grepl((Precision)
31. Recall (F1)→ names(byClass))]
32. overallText <- c(overallText,format(byClass, digits = digits))
33. FP (overallNames, names(xbyClass))
34. ifelse(overallNames == (overallNames))
35. TP (overallNames,Positive, Class)
36. overallText <- c(overallText, xpositive)
37. out <- cbind(format(overallNames, justify =right), overallText)
38. colnames(out) <- rep(ncol(out))
39. rownames(out) <- rep(nrow(out))
40. out <- rbind(out, rep(2))
41. out, quote = FALSE
42. invisible(x)

IMAGE ACQUISITION

Magnetic resonance imaging was completed at baseline and 10 weeks. Data Received on 3D General Electric ASA image Scanner with eight channel head coil. Imaging protocols include: (1) an axis T1-weighted 3D inverse retrieval-ready fast corridor echo array (echo time (TE) = .8 ms, repetition time (TR)) 9.9 ms, reverse time = 766) Ms,) bend angle = 15. Bottom, acquisition matrix = 320 × 320, 222 pieces, field of view = 256 mm, slice thickness = 0.8 mm, tone size = 0.8 × 0.8 × 0.8 mm 3).UCI Data set processing NIAK 2020 four single vowel point spectroscopy (PRESS) acquisition (TE = 20 ms, TR = 1300 ms, life size = 200 × 200 × 100 mm 3, True negative 149 number of means in right and left strips, and 128 for evaluation of living characters in right and Left lateral cortex) was used. The maximum amount of gray matter and the minimum amount of cerebrospinal fluid were added. Flashing ADD to reach full-width half-maximum (line width DSM-IV of Hz= 3) resting position. Functional versions were obtained using a gradient echo array (TE = 35 ms, TR = 2500 ms, FA = 15 °, acquisition matrix = 64 × 64, FOV = 240 mm, 36 pieces, etc.). 160 Again, life size = 3.75 × 3.75 × 3.8 mm3 , Scan time = 8:10). During fMRI acquisition[5], participants were asked to lie down and relax while focusing on a certain intersection.

PROBLEM

This particular diagnosis of developmental disorder was all children with Asperger's disease diagnoses (ADD) using the DSM-IV criteria for autism and AS. All children met DSM-IV criteria for autism.There is no general logic and confidence in poor reliability transparency all patients' results.

FMRI PROCESSING

An electroencephalogram signal is a measure of flow to the brain. These indicators are the smallest in the microvolt range and differ from the hemisphere. Up to about half the rays, these signals receive electrodes in the form of joints around the skull and act as ground through the ADD. Depending on the performance of the brain, signal areas such as thought, hearing, sleep and acceleration vary. Because of its very small amplitude, this signal is sensitive to noise such as an fMRI. These fields should be deleted. Before looking at the paging signal, the signal is designed to eliminate unwanted noises. Resources are extracted and presented to the classifier[6] to indicate whether the article is subject to ASD. By comparison, it is a cheaper method and takes less time.

This method fMRI harmful rays noise levels, but depends on the quality of the electrodes used. The equipment is inexpensive, easy to handle and easy to transport. Researchers encourage this small, well-established method. This method reduces the cost of scanning and helps identify patients at an early stage.

DATASET PROCESSING FMRI

Patient generic FIR signals were obtained from the Autistic Spectrum Disorder Screening Data for Children Data Set in UCI repository. This is called NIAK Match IV (dataset 1). HH was obtained from Horizon 2020.We looked at general patient data and the autistic brain image L10 dataset for autistic patients. The resulting data set was sampled at 256 Hz. Realistic HFA for autistic and non-autistic individuals. As seen in both figures[7], the typical object has a frequency of 100 Hz and is within a certain wavelength pattern.

The non-autistic frequency range is up to 100 Hz and the amplitude is random. Random waveform pins indicate that neurons cannot understand this CNN. There are differences in the voltage level so that the signal is correct[8].

Table 1 : Data set of age of autistic patients groups

Age Groups	0-4 Age	5-9 Age	10 – 14 Age	15 – 17Age	18+
Autism	23	33	34	34	12
ASD	111	122	34	23	32
PDD-NOS	23	34	34	44	32
All	**157**	**189**	**102**	**111**	**76**
Total	**157+189+102+111+76**				**635**

We need to use inputs (G) that protect space in both frequency $\pm\delta_p$ and time axes ASD equation (1 to 3) groups .

$$\left|LG(e^{j\omega})\right| \le \delta_s, \quad \omega_s \le |\omega| \le \pi \quad \text{..... (1)}$$

$$\omega_s \le \omega \le \pi \qquad \pm \delta_p \quad \text{..... (2)}$$

$$\left|LG(e^{j\omega})\right| \cong 0 \qquad \text{--+} \delta_s \quad \text{..... (3)}$$

Time: presents no immediate problem from the point of view of location(ω_p) . Like other Thickness for neuron , CNN will have a wider context (9–15 frames) in the input equation (4 to 6) window.

$$0 \le \omega \le \omega_p \quad \text{..... (4)}$$

$$1-\delta_p \le \left|LG(e^{j\omega})\right| \le 1+\delta_p, \quad |\omega| \le \omega_p \quad \text{..... (5)}$$

$$\mathrm{LG}(\omega) = -20\log_{10}\left|LG(e^{j\omega})\right| \qquad \text{DB} \quad \text{..... (6)}$$

In this article, we will use the calculated energy directly from the speed Frequency Spectral Image (7 to 8) without CNN (α_p), we will display as the HFA properties $(1-\delta_p)$.

$$\alpha_p = -20\log_{10}(1-\delta_p) \quad \text{..... (7)}$$

$$\alpha_s = -20\log_{10}(\delta_s) \quad \text{..... (8)}$$

Frequency: The traditional use of NASDA presents a major problem because the discrete cosine (ω_p) converts the project's frame Connectivity and thickness equation (9 to 10) into a new base that may not be able to sustain its terrain

$$\omega_p = \frac{\Omega_p}{F_T} = \frac{2\pi F_p}{F_T} = 2\pi F_p T \quad \text{..... (9)}$$

$$\omega_s = \frac{\Omega_s}{F_T} = \frac{2\pi F_s}{F_T} = 2\pi F_s T \quad \text{..... (10)}$$

HFA features will be used to represent each delta and delta delta, as well as the frame of each speech (to describe the distribution of sound energy in several different frequency bands.

$$\omega_p = \frac{2\pi(7\times10^3)}{25\times10^3} = 0.56\pi \quad \text{.... (11)}$$

$$\omega_s = \frac{2\pi(3\times10^3)}{25\times10^3} = 0.24\pi \quad \text{..... (12)}$$

There are several different options for managing these HFA features in the CNN map. They can be configured as three 2-D feature maps, each representing features Extraction (constant, delta, and delta delta) that are used by frequency FIR (Equation (13) using frequency band index) and time. HH filter represents the frame number used within the window).

$$H(z) = \frac{p_0 + p_1 z^{-1} + p_2 z^{-2} + \cdots + p_M z^{-M}}{d_0 + d_1 z^{-1} + d_2 z^{-2} + \cdots + d_N z^{-N}} \quad \text{..... (13)}$$

In this case, the Three dimensional (equation 14 to 16) determination is to normalize both the frequency and the temporal patterns H(z) simultaneously.

$$H(z) = \sum_{n=0}^{N} h[n]\, z^{-n} \quad \text{..... (14)}$$

$$H(z) = h_0 + h_1 z^{-1} + h_2 z^{-2} + \ldots + h_n z^{-n} \quad \text{..... (15)}$$

$$H(z) = K \prod_{i=1}^{n_1} (1 - \alpha_i z^{-1}) . \prod_{i=1}^{n_2} (1 - \beta_i z^{-1}) \quad \text{..... (16)}$$

Alternatively, we can consider normalizing the frequency shift only. Accuracy, speed ,Reliability HH the reference window has 15 frames and 40 frame is used for each frame, we will create 45 (ie, 15 times 3) 1-D feature maps, each map is 40 dimensions Filter FIR.

$$s_f = \frac{1}{n}\left(| x_{1f} - m_f | + | x_{2f} - m_f | + \ldots + | x_{nf} - m_f | \right), \quad \text{... (17)}$$

$$m_f = \frac{1}{n}\left(x_{1f} + x_{2f} + \ldots + x_{nf} \right), \quad \text{... (18)}$$

$$z(x_{if}) = \frac{x_{if} - m_f}{s_f}. \quad \text{.... (19)}$$

$$dist(\mathbf{x}_i, \mathbf{x}_j) = \frac{\sum_{f=1}^{r} \delta_{ij}^{f} d_{ij}^{f}}{\sum_{f=1}^{r} \delta_{ij}^{f}} \quad \text{... (20)}$$

$$entropy(D) = -\sum_{j=1}^{|C|} \Pr(c_j) \log_2 \Pr(c_j) \quad \text{... (21)}$$

$$\text{chance correct decision 2 - AFC exp.} = \int_{-\infty}^{\infty} dx\, P_n(x) \int_{x}^{\infty} dx'\, P_p(x')$$

$$A_z = \int_{-\infty}^{\infty} dx\, P_n(x) \int_{x}^{\infty} dx'\, P_p(x') \quad \text{.... (22)}$$

ALGORITHM

(1) We trained the fragments of image total 635 patient split test and training formation steps CNN progressed to the background and ASD and Amygdala torsion, respectively.

(2) First, trained NIAK 2020 and only pre-processed FMRI volume is tested(80%) and training(20%) in Accuracy with combined with the message of the stacked volume of peppermint is the message and the biggest area above ASD patient neuron thickness.

(3) The ADD feature map, the compromised operation can be considered a simple matrix multiplication, and the right image is a small sparse matrix W, obtained by combining the original matrix with the left matrix.

(4) The original matrix W on the left has a local weight matrix[9] wedge, with an I * F row (45 I * filter size 5), and 1 frequency in each frequency band (since it contains Max pooling input feature maps Huh. Then J is the column. The input feature map and the convolution feature map can be calculated as row vectors A and Q.

(5) The single row vector O is to traverse all ASD input feature maps, and then they are all combined. Recall is an array vector, representing the F1 Score frequency band from all I input feature maps.

(6) The expressed as a line vector multiplied by a weight vector and then subjected to the sigmoid operation, which is a commonly hidden layer of the preceding amygdala.

(7) New methods uses HFA for pre-training to improve performance, especially when the training set is small. will allow the weight of Amygdala to begin and the weight to reach a reasonable range, so that correction and normalization will have a better effect.

(8) The CNN treats each set of hidden units in the pool as a multidimensional distribution, and each group of pools will have at least one unit moving. Therefore it is necessary to be confident on voting when there is no overlap[11] to assure Frames using weight sharing Amygdala.

PRE-PROCESSING

For Amygdala and Amygdala a distribution, FMRI images of formats contain much unnecessary information. Usually, a defined range (Christ et al., 2016) is used to truncate the gray scale to exclude unrelated instruments and objects. However, this constant region is not the same for all data with different contrast injection and image acquisition. In this work, we use the open source software, Amira (Stalling et al. 2005), to convert images from DICOM or NIAK to BMP format. Gray scale by automatically and automatically adjusting a gray[11] area histogram(fig: 2) to FIR change map pixel spited parameters ranges of framesets .

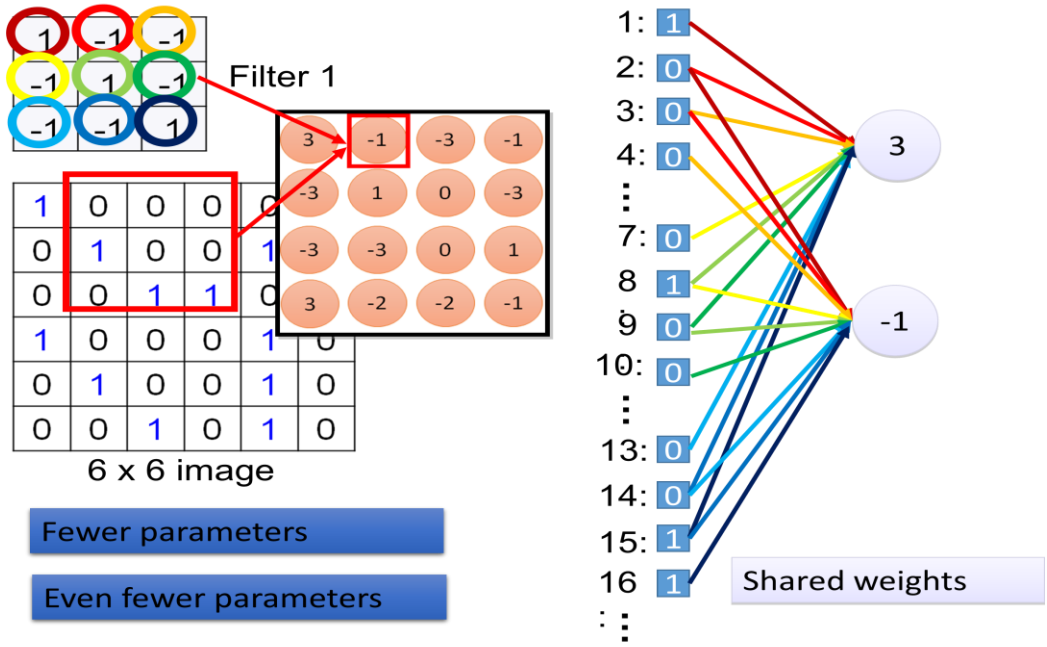

Fig 2: Convocation assuming filter FIR size of 45 input feature map and 80 feature map.

Compared to the amygdala format and the JPEG require a smaller storage space and it is more convenient to browse a computer. As can be seen in Figure 2 (a, b). CNN images contain less irrelevant organs and objects, such as abdominal fat, that contribute to the study of patterns[12]. So, the simplest pre- treatment on FMRI images is the following steps using the training step. First, the images were converted to the original DICOM format JPEG images. Second, the autistic brain image FMRI images were pre-processed by FIR and HH to improve the signal-to-noise ratio and enhance spatial resolution. Third, the pre-processed images were downgraded by a factor of 2 to train the models. The fragmentation step was performed by the same pre-treatment and sampling procedure.

IMPLEMENTATIONS

The data used has two general 3D databases FIR and HH filter level of increase to changes of current accuracy and speed. The 3D database[13] belonging to the FIR autistic brain image contains 3D FMRI scans. In 75% of cases (15 cases), 10 women and 10 men have Amygdala Neuron. The database contains anonymous image of the patient, tag ASD associated with various tissues and classified shape to quantify Neuron Anaysis in the form of . The NIAK database is provided to encourage the researcher to develop

automated segmentation methods to assign Amygdala shape to quantify Neuron Analysis ASD with or without CNN differential enlargement.

Abdominal FMRI scan. The database contains 149 FMRI exams and 70 FMRI exams. Training data were labelled as Amygdala area, brain, background. This challenge has been organized in collaboration ASD. The data and fragments of these two databases were manually created by radiologists[14] from various medical sites around the world, working in pieces. FMRI scans of these two datasets differ significantly between Brain variability, number and size. All FMRI modules have a resolution of 512 to 512 pixels and contain several pieces ranging from 64 to 987 pixels. The distance of the inner pixels ranges from 0.56 to 1 mm and the distance between the pixels (strip thickness) varies from 0 to 7 and 5.0 mm.

During the training phase(Table:1) , the CNN model requires a large number of training images. 131 Training All 499 image pieces of the chess board are used for a well-trained sample. Next, the HFA dataset is used for testing, assuming that the data are consistent with the different[15] training data (because the 70 lids are not comparable to the ASD selection because the actual land measurement is not available.

EXECUTION PROCESSING HFA FULL CONNECTED

Different HFA Binary models can be used to estimate future separation values Distance and location. In addition to the technology used to create the models(fig 3) important to correctly select the input variables H_z. Three approaches have been used Develop forecast templates that focus on predicting the future values of a time series Current and Past Observations. Neuron is achieved in a period known as lead better results of convolution.

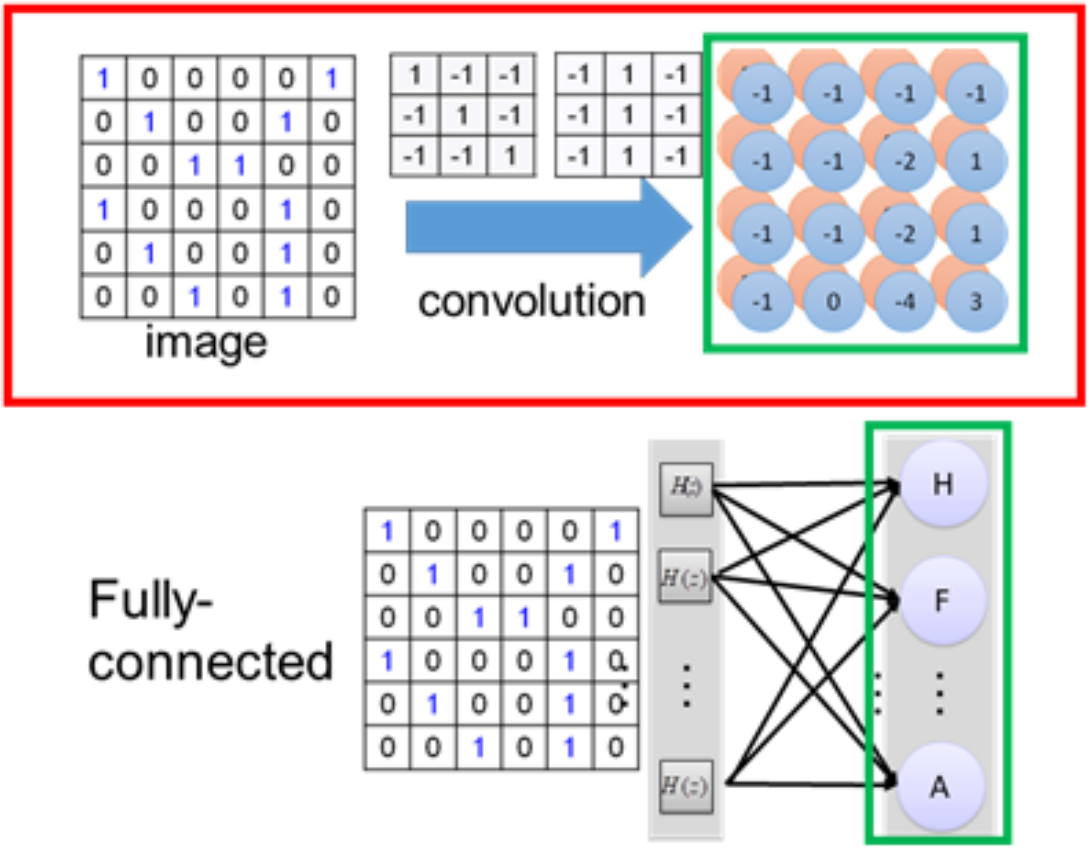

Fig 3: Fully connected HFA Time seconds processing

The time is set to 5, 10, 15, 20, 25 and 30 seconds for this particular time [16]Application. As delivery time increases. On the other hand, increasing wakefulness time allows you to create alarms Previous.

DESCRIPTIVE STATISTICS AND RESULTS

We performed a descriptive analysis using internal Connectivity and thickness data with the New methods algorithm, which divides 149 segments into 20 Connectivity and thickness. Interestingly[17], the autistic

brain image pattern Classification Connectivity and thickness had 93 options (66% of the total), while the others were distributed among the Connectivity and thickness (fig.4) On the autistic brain image pattern Classification Connectivity and thickness concentrating, 149 mainly consisted of sex, lesions, and functions options. The men and women in the group were well balanced (53 men and 40 women). Instead, the original type is not evenly distributed with staples spilit True positive (TP) and True Negative(TN) .

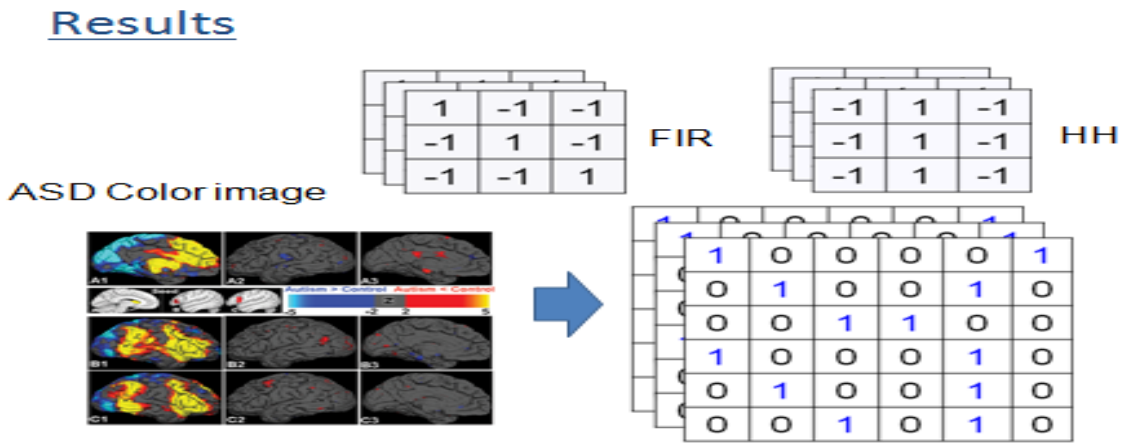

Fig 4: ASD colour image Max Pooling methods binary neuron thickness

All Connectivity and thickness (fig.5) of the total: nerve (1/3, 33%), vascular (11/25, 44%), alcoholic (3/5, 60%), cortical (2/3, 67%) and broad (76/105)). , 72%). Notably, all tasks were predominantly in group 24: left finger tapping (14/26, 54%), object naming (19/31, 61%), right finger tapping (16/25, 64%) , And verb formation (19). / 29, 66%), visual processing (2/3, 67%), verbal fluency (22/26, 85%), and sentence mining (1/1, 100%). As a result, the rate of examinations performed by tasks will always exceed 50% of the total, rather than the proportion of the most heterogeneous lesions between them.

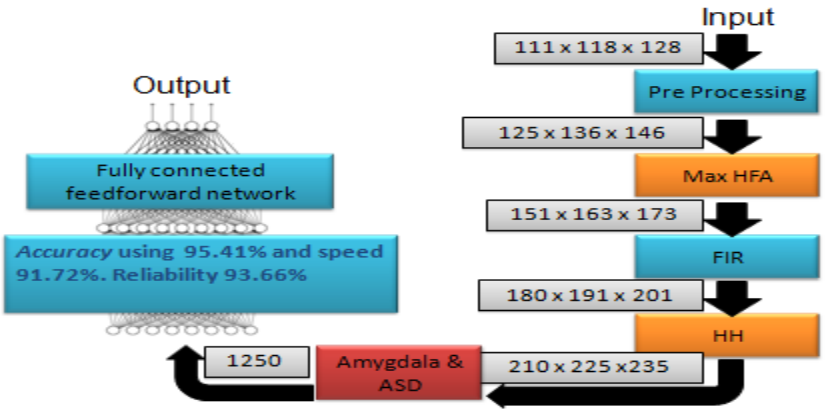

Fig 5: Amygdala Connectivity and thickness step to step processing

Finally, the autistic brain image pattern Classification Connectivity and thickness of examinations consisted mainly of extensive ulcers (76/105, 72% total) and oral fluency tasks (22/26, 85% of the total). In particular, the only selection characterized by brain connectivity is included in the amygdale Connectivity and thickness.

Table 2 : ASDA Connectivity and Thickness

	True Positive	True Negative
Predicted Positive	499	20
Predicted Negative	18	149

Table 3: Amygdala Connectivity and thickness step to step processing Results

Measure	Value	Percentage	Derivations
Sensitivity	0.9652	96.52%	TPR = TP / (TP + FN)
Specificity	0.8817	88.17%	SPC = TN / (FP + TN)
Precision	0.9615	96.15%	PPV = TP / (TP + FP)
Negative Predictive Value	0.8922	89.22%	NPV = TN / (TN + FN)
False Positive Rate	0.1183	11.83%	FPR = FP / (FP + TN)
False Discovery Rate	0.0385	3.58%	FDR = FP / (FP + TP)
False Negative Rate	0.0348	3.48%	FNR = FN / (FN + TP)
Accuracy	0.9446	94.46%	ACC = (TP + TN) / (P + N)
F1 Score	0.9633	96.33%	F1 = 2TP / (2TP + FP + FN)
Matthews Correlation Coefficient	0.8503	85.03%	TP*TN - FP*FN / sqrt((TP+FP)*(TP+FN)*(TN+FP)*(TN+FN))

Amygdala with FMRI in ASDA : repetitive / restrictive interests and behaviors, including social impairments, communication deficits, and emotional abortion. The observed behavior is evaluated through several types of practical studies. Depending on the observer's clinical judgment and the child's age, developmental status amygdala and restrictions. After an interval between the inspector and the child (fig 6)the inspector rated each item on a 3-point alcohol scale: 0: no reduction. 1 light loss; 2 severe air shortages[18]. Some things include: When the name is called autistic brain image, when asking for help, facial expressions, strange body. Posture and 'extraordinary lust in the moving object'. Examiners should have at least experience with ASD symptoms. ASD management examines trained doctoral level graduate students as For ASD Cronbach's alpha for this study has the highest internal consistency of 0.96 and good inter-router reliability (96.33%). ASDA examined the joint validity of the move and found that ASD was important.

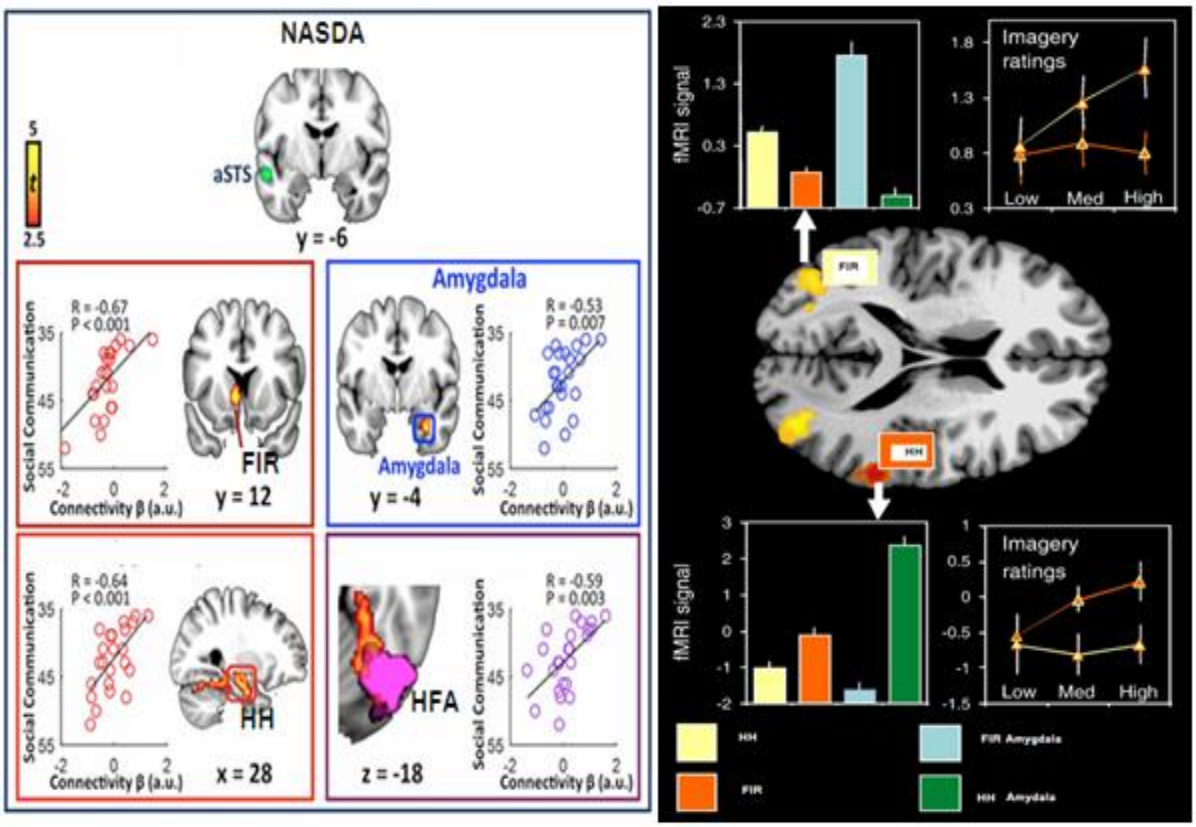

Fig6: This measure includes items assessing all of the key features of ASDA

ROC CURVE

In a sense, sensitivity and specificity are more interesting measures than accuracy because they do not depend on the previous distribution of negatives and positives in the test database. Sensitivity is only

calculated from positive cases, and the detection rate algorithm is only negative cases from the calculated count, and the chance of a false alarm is zero. Receiver operating character curve Accuracy. After originally proposed in radar detection theory with Formalizes the trade-off between sensitivity and specificity call recall. Clarifies discrimination and decision bias Each hard classifier is an ROC(fig 7) curve at an operating point single-sized performance system is the ROC curve under that area A system that randomly generates a label with the ROC curve at probability p, which is a straight line (0,0) to (1,1), ass = 0.5 = 1 in a perfect setting Ass is not dependent on the previous probability (diffusion)

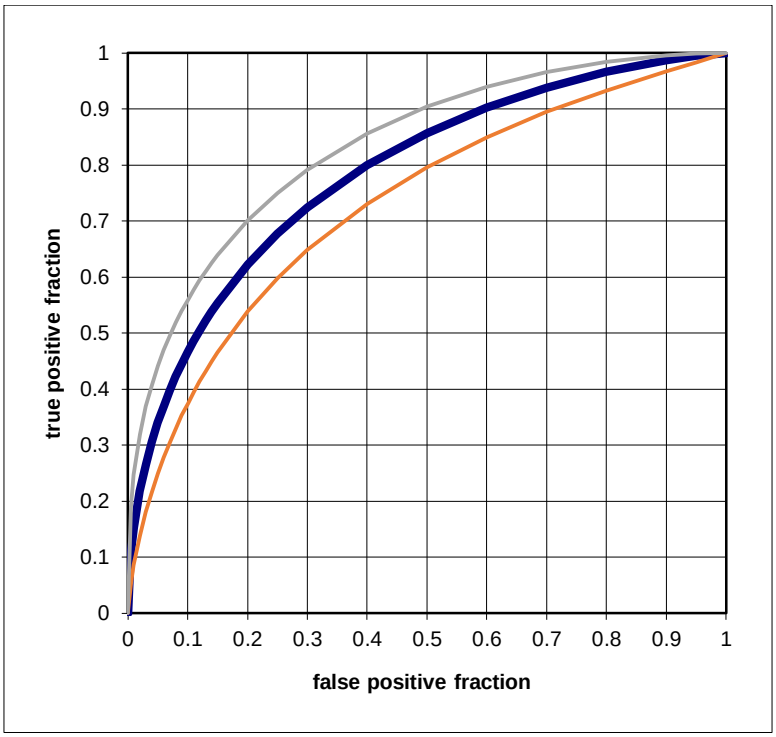

Fig 7: Connectivity and thickness ROC Curves

If one assumes that True and False are Gaussian, then there are two parameter curves. The difference between the means and the standard deviation. They can be estimated by the maximum likelihood procedure. There are two ROV curves for obtaining confidence intervals for ROC curves and procedures.

CONCLUSION

Regarding mass data analysis, it should be noted that while clustering may prove to be a flexible tool for fMRI analysis, there are some limitations. These methods cause different mechanisms to trigger different topologies, and different configurations of the same method may give different results. There is a need to understand the proposed mechanism of multiple runs. Parameter and initialization conditions vary. The test brain ASD allowed the use of a NIAK 2020 Datat Set representation to achieve reliable, consistent results in combination with a good algorithm. As a future work, the autistic brain image pattern Classification Connectivity and thickness of peculiar facility systems proceeds to deepen analysis of its contents. For statistical purposes, to analyze multivariate analysis, examiner similarities and differences in group (0 to 18+) data set and others in a different group, and hypotheses between groups and clinical features, brain function information, areas of interest, and related codes for four testing. ADD is a semi-structured surveillance measure used to evaluate autistic pathology. Another ASD is associated with a surveillance measure (the Childhood Autism Rating Scale) (R 0. 0.83). H DSM-IV, Children with ASD symptoms are more severe than those diagnosed earlier. DSM-IV no longer receives ASD diagnostics, which allows for service availability. Children are suspicious. Future these concept findings raise concerns about the proposed change in CNN criteria and should be considered with other collaborative research in preparation best results of reliability 96.33%.

REFERENCE

1. Zhang J, Xia Y, Xie Y, Fulham M, Feng D. 2017. Classification of medical images in the biomedical literature by jointly using deep and handcrafted visual features. IEEE J Biomed Health Inform. PP(99): 1–11.
2. Stalling D, Westerhoff M, Hege HC. 2005. Amira: a highly interactive system for visual data analysis. Visualization Handb. 27:749–767.
3. To cite this article: Shenhai Zheng, Bin Fang, Laquan Li, Mingqi Gao, Yi Wang & Kaiyi Peng (2019): Automatic Amygdala Neuron segmentation in FMRI combining FCN and NMF-based deformable model, Computer Methods in Biomechanics and Biomedical Engineering: Imaging & Visualization,DOI: 10.1080/21681163.2018.1493618
4. Ramona Toscano, Andrew J. Baillie, Heidi J. Lyneham, Anna Kelly, Theresa Kidd, Jennifer L. Hudson,Assessment of anxiety in children and adolescents: A comparative study on the validity and reliability of the Spence Children's Anxiety Scale in children and adolescents with anxiety and Autism Spectrum Disorder, Journal of Affective Disorders,Volume 260, 2020,Pages 569-576,ISSN 0165-0327,https://doi.org/10.1016/j.jad.2019.09.055.
5. Lucie Bellalou, Emilie Cappe,Trouble dépressif et trouble du spectre de l'autisme chez l'enfant et l'adolescent : analyse de la portée de la littérature depuis la parution du Manuel diagnostic et statistique des maladies mentales 5 (DSM 5),Journal de Thérapie Comportementale et Cognitive,Volume 29, Issue 2,2019,Pages 82-92,ISSN 1155-1704,https://doi.org/10.1016/j.jtcc.2018.11.002.
6. Danielle A. Baribeau, Simone Vigod, Eleanor Pullenayegum, Connor M. Kerns, Pat Mirena, Isabel M. Smith, Tracy Vaillancourt, Joanne Volden, Charlotte Waddell, Lonnie Zwaigenbaum, Teresa Bennett, Eric Duku, Mayada Elsabbagh, Stelios Georgiades, Wendy J. Ungar, Anat Zaidman-Zait, Peter Szatmari,Repetitive Behavior Severity as an Early Indicator of Risk for Elevated Anxiety Symptoms in Autism Spectrum Disorder, Journal of the American Academy of Child & Adolescent Psychiatry,2019,ISSN 08908567, https://doi.org/10.1016/j.jaac.2019.08.478.
7. Shubhangi Nema, Akshay Dudhane, Subrahmanyam Murala, Srivatsava Naidu,RescueNet: An unpaired GAN for brain tumor segmentation,Biomedical Signal Processing and Control,Volume 55,2020,101641,ISSN 1746-8094,https://doi.org/10.1016/j.bspc.2019.101641.
8. Nitin Agarwal, Xiangmin Xu, M. Gopi,Geometry processing of conventionally produced mouse brain slice images,Journal of Neuroscience Methods,Volume 306,2018,Pages 45-56,ISSN 0165 0270,https://doi.org/10.1016/j.jneumeth.2018.04.008.
9. Chin-Po Chen, Susan Shur-Fen Gau, Chi-Chun Lee,Toward differential diagnosis of autism spectrum disorder using multimodal behavior descriptors and executive functions,Computer Speech & Language,Volume 56,2019,Pages 17-35,ISSN 0885-2308,https://doi.org/10.1016/j.csl.2018.12.003.
10. Benjamin E. Yerys, Jennifer R. Bertollo, Juhi Pandey, Lisa Guy, Robert T. Schultz,Attention-Deficit/Hyperactivity Disorder Symptoms Are Associated With Lower Adaptive Behavior Skills in Children With Autism,Journal of the American Academy of Child & Adolescent Psychiatry,Volume 58, Issue 5,2019,Pages 525-533.e3,ISSN 0890-8567,https://doi.org/10.1016/j.jaac.2018.08.017.
11. Kristina Safar, Veronica Yuk, Simeon M. Wong, Rachel C. Leung, Evdokia Anagnostou, Margot J. Taylor,Emotional face processing in autism spectrum disorder: Effects in gamma connectivity,Biological Psychology,2019,107774,ISSN 0301-0511, https://doi.org/10.1016/j.biopsycho.2019.107774.
12. Kwok-Wai Hung, Wan-Chi Siu,Single-image super-resolution using iterative Wiener filter based on nonlocal means,Signal Processing: Image Communication, Volume 39, Part A,2015,Pages 26-45,ISSN 0923-5965, https://doi.org/10.1016/j.image.2015.07.003.
13. He Chen, Yan Song, Xiaoli Li,A deep learning framework for identifying children with ADHD using an EEG-based brain network,Neurocomputing,Volume 356, 2019,Pages 83-96,ISSN 0925-2312, https://doi.org/10.1016/j.neucom.2019.04.058.
14. Ekaterina Ostashchenko, Gaétane Deliens, Stephanie Durrleman, Mikhail Kissine, An eye-tracking study of selective trust development in children with and without autism spectrum disorder,Journal of Experimental Child Psychology,Volume 189,2020,104697,ISSN 0022-0965,https://doi.org/10.1016/j.jecp.2019.104697.
15. Erin Robinson, Laura Hull, K.V. Petrides,Big Five model and trait emotional intelligence in camouflaging behaviours in autism,Personality and Individual Differences,Volume 152,2020,109565, ISSN 0191-8869, https://doi.org/10.1016/j.paid.2019.109565.

16. Peter Vuust, Leif Ostergaard, Karen Johanne Pallesen, Christopher Bailey, Andreas Roepstorff,Predictive coding of music – Brain responses to rhythmic incongruity,Cortex,Volume 45, Issue 1,2009,Pages 80-92,ISSN 0010-9452,https://doi.org/10.1016/j.cortex.2008.05.014.
17. Susan Faja, Tessa Clarkson, Sara Jane Webb,Neural and behavioral suppression of interfering flankers by children with and without autism spectrum disorder,Neuropsychologia,Volume 93, Part A,2016,Pages 251-261,ISSN 0028-3932,https://doi.org/10.1016/j.neuropsychologia.2016.10.017.
18. Vilayanur S. Ramachandran, Zeve Marcus, Chaipat Chunharas, Chapter 1 - Bouba-Kiki: Cross-domain resonance and the origins of synesthesia, metaphor, and words in the human mind,Editor(s): K. Sathian, V.S. Ramachandran, Multisensory Perception,Academic Press, 2020,Pages 3-40,ISBN 9780128124925, https://doi.org/10.1016/B978-0-12-812492-5.00001-2.